Impact of Control Allocation Methods on the Design of Control Surface Layouts for Box-Wing Aircraft under Flying Qualities Constraints

Wahler, N.F.M.; Varriale, Carmine; la Rocca, G.

DOI
10.2514/6.2023-3485

Publication date
2023

Document Version
Final published version

Published in
AIAA AVIATION 2023 Forum

AIAA AVIATION Forum
12-16 June 2023, San Diego, CA and Online
AIAA AVIATION 2023 Forum

10.2514/6.2023-3485

Impact of Control Allocation Methods on the Design of Control Surface Layouts for Box-Wing Aircraft under Flying Qualities Constraints

Nicolas F. M. Wahler *
University of Southampton, Southampton, SO16 7QF, United Kingdom

Carmine Varriale †, Gianfranco La Rocca ‡
Delft University of Technology, Delft, 2629 HS, The Netherlands

This paper compares optimum control surface layouts designed and sized to obtain the same Flying Qualities (FQs) performance with different Control Allocation (CA) methods, and proposes novel layouts for staggered box-wing aircraft aimed at transonic commercial flight. Box-wings allow the installation of redundant control surfaces for which no explicit role can be defined a priori, but present challenges related to aerodynamic interaction and interference effects. To evaluate the impact of different CA methods on top-level layout parameters, the cumulative control surface span and the properties of the Attainable Moment Set (AMS) corresponding to each control surface layout are used. A physics-based multi-disciplinary optimization framework is developed to size the control surface layout. FQs are evaluated through non-linear flight dynamics simulation, using a variable-architecture flight control system that allows their assessment as a function of different CA methods. The most traditional Mechanical Gearing and Ganging (MGG) approach, the Constrained Pseudo-Inverse (CPI) method and the Direct Control Allocation (DCA) method are compared. Results show that different optimum layouts exist with comparable cumulative span, for a given CA method and same FQs requirements. The traditional MGG approach requires the largest cumulative control surface span, but retains the best ability to generate coupled roll-pitch moments. DCA requires the smallest cumulative control surface span, with the largest AMS volume. By using this method, a novel layout featuring a mid-wing rear elevon has been discovered, which reduces the total required control surface span by about 13%, results in a 3.7% increase of span available for flaps on the front wing, and avoids detrimental aerodynamic interaction effects near the wing-tail intersection region.

Nomenclature

Roman letters

a	resultant acceleration, $\mathrm{m/s^2}$
B	control effectiveness matrix, $1/\mathrm{rad}$
C	dimensionless coefficient
F	generic force or moment, N or N m
f	generic function
G	ganging matrix
h	altitude, m
$\mathcal{L}$	roll moment, N m
m	mass, kg
M	Mach number
$\mathcal{M}$	pitch moment, N m
N	number of elements
n	load factor
$\mathcal{N}$	yaw moment, N m
p	roll rate, rad/s
q	pitch rate, rad/s
r	yaw rate, rad/s
t	time, s
u	control input
V	airspeed, m/s

Greek letters

α	angle of attack, rad

*Ph.D. Candidate, Department of Aeronautics and Astronautics, Faculty of Engineering and Physical Sciences, n.f.m.wahler@soton.ac.uk.
†Assistant Professor, Flight Performance and Propulsion Section, Faculty of Aerospace Engineering, C.Varriale@tudelft.nl.
‡Associate Professor, Flight Performance and Propulsion Section, Faculty of Aerospace Engineering.

β angle of sideslip, rad
δ control surface deflection, rad
η non-dimensional spanwise position
ν control objectives
ω angular rate, rad/s
φ roll angle, rad

Subscripts and superscripts

lb lower bound
tr trim condition
ub upper bound

I. Introduction

With the seemingly unstoppable growth in passenger demand, the increasing ecological awareness, and the ever more stringent requirements imposed by institutions and regulators, it has become imperative for the global aviation industry to invest in research and development of more environmentally sustainable solutions [1–3]. As the conventional tube-and-wing aircraft configuration is believed to have reached its technological limit [4–6], the attention of researchers has recently shifted towards innovative airframe concepts. In these regards, aircraft configurations employing a (staggered) box-wing geometry have enjoyed revived scientific interest [7–10].

By using two full-size wings connected at the tips to create a closed shape, the box-wing concept can achieve the lowest possible induced drag for a given span and weight [11–13]. This translates to significant performance benefits in the short-to-medium flight range, where climb and descent phases constitute a larger fraction of the total mission profile, and the box-wing low-speed performance benefits can be exploited more proficiently [14, 15].

The double-wing architecture of box-wing aircraft can also accommodate more Control Surfaces (CSs) than strictly required for basic controllability, as shown in Figure 1. The additional design space available for positioning and sizing CSs has been explored in only a few research studies [16–19]. In all of these, each CS is explicitly assigned a specific role as elevator or aileron, hence responding only to pitch or roll commands, respectively. This is equivalent to imposing an arbitrary mechanical Flight Control System (FCS), which gangs CSs together and links them to the pilot input with predefined gearing ratios.

For such a set of redundant CSs, spreading over both wings fore and aft of the aircraft Center of Gravity (CG), the control function of each one of them does not need to be fixed a priori. For example, an outboard surface on the rear wing can be used for roll control as well as for pitch control, due to its significant longitudinal distance to the aircraft

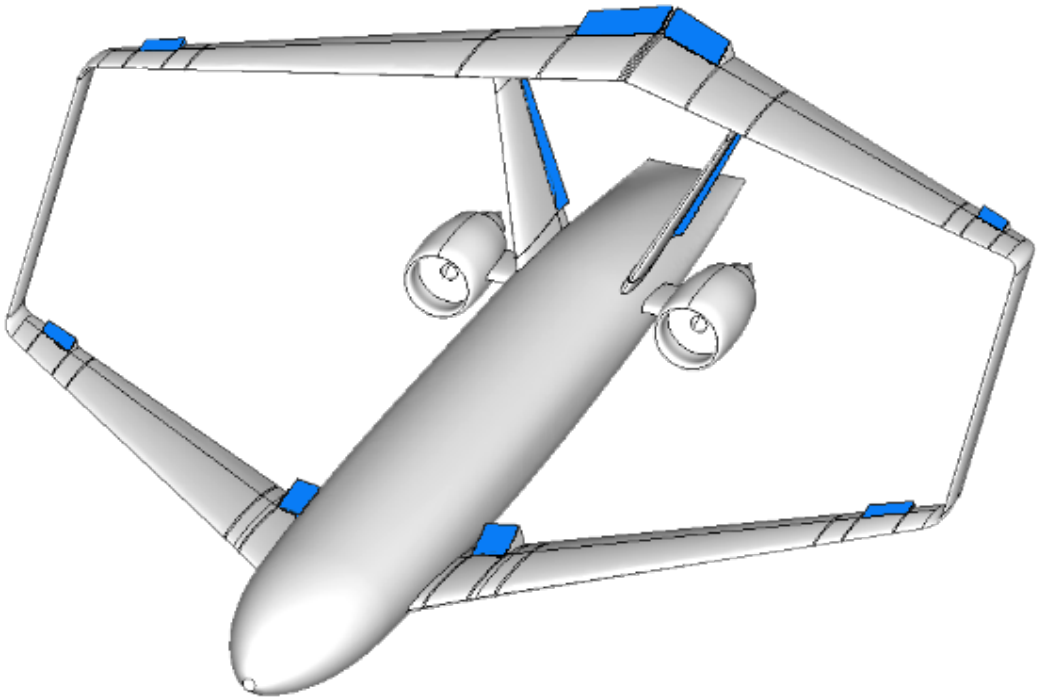

Fig. 1 Box-wing aircraft configuration with highlighted control surfaces.

CG. This flexibility should be exploited to improve the flying and handling qualities characteristics of the aircraft. Redundant CSs can be coordinated to increase safety in case of failure, actively control the aerodynamic load over the wing, and allow innovative techniques in maneuvering flight, such as direct lift control [20–22]. A possible way to do so is through the employment of Control Allocation (CA) methods.

CA methods allow the FCS to find the best combination of CS deflections resulting in the generation of aerodynamic control forces and moments required by pilot or auto-pilot commands. CA methods exploit all available CSs at the same time, and utilize them independently on the basis of their respective aerodynamic effectiveness. By employing CA methods, assigning a predetermined role to each CS is not necessary anymore, since each CS can contribute to various aircraft control tasks in the best way allowed by its effectiveness [23]. This advantage should also be taken into account at the stage of aircraft conceptual and preliminary design, as it may lead to improved CS layouts, and related weight and performance benefits.

This paper compares optimum CS layouts obtained with different CA methods under the same flying qualities constraints, and evaluates novel CS layouts for the rear wing of staggered box-wings. The volume and shape of the Attainable Moment Set (AMS) corresponding to each CS layout are used as criteria to evaluate the impact of different CA methods on top-level layout parameters. The following CA methods are investigated: a traditional Mechanical Gearing and Ganging (MGG) approach, as a benchmark for comparison with available literature, the Constrained Pseudo-Inverse (CPI) method, as a sub-optimal method, and the Direct Control Allocation (DCA) method, as an optimal one.

A first study focuses on the minimum total CS span required by an aircraft model to achieve desired Flying Qualities (FQs). For this study, the position of the movable surfaces on the wings is predetermined on the basis of current state-of-the-art CS layouts for box-wings. A second study is performed by using the DCA method to evaluate novel CS layouts for the rear wing. The purpose of this study is to explore the possibility of leaving the region between the vertical tails free, in order to avoid aerodynamic interference effects due to the complex aerodynamic flow in that area and promote ease of accessibility to movables.

The fundamental theory of CA methods is outlined in the following Section II. The optimization framework developed to perform the CS sizing iteration and evaluate the flying qualities constraints is presented in Section III. Results from the CS sizing iterations using different CA methods are compared in Section IV.A. The newly explored CS layouts for box-wings are reported in Section IV.B. Conclusions and recommendations are provided in Section V.

II. Background

CA methods calculate the optimal combination of CS deflections necessary to perform a given maneuvering task. In general, they define an analytic or algorithmic function f_{CA} to calculate the optimal effectors displacements $\boldsymbol{u}$ that obtain the required control objectives $\boldsymbol{\nu}$, on the basis of the available effectiveness B and, optionally, other flight or design parameters [24]. The fundamental CA problem is expressed in Equation 1, and its generic solution in Equation 2.

$$B\boldsymbol{u} = \boldsymbol{\nu} \tag{1}$$

$$\boldsymbol{u} = f_{\mathrm{CA}}(B, \boldsymbol{\nu}, \dots) \tag{2}$$

The control effectiveness matrix B expresses the influence that each control surface has on each control objective. Reference values for $\boldsymbol{\nu}$ are typically the output of the control law, and most commonly represent control forces and moments, as well as angular rates. If $\boldsymbol{\nu}$ is an array of control forces and/or moment coefficients to be generated by the effectors, B is defined as in Equation 3.

$$B = \frac{\partial \boldsymbol{C_F}}{\partial \boldsymbol{u}} = \frac{\partial C_{F_i}}{\partial u_j} \quad \forall i = 1, \dots, N_{\boldsymbol{\nu}}, \;\; \forall j = 1, \dots, N_{\boldsymbol{u}} \tag{3}$$

The B matrix defines a linear map between the set of allowed positions of the effectors, referred to as the Admissible Controls Set (ACS), to the set of control forces and moments that can be generated by them, here referred to as the Effective Moment Set (EMS). If the ACS is a bounded convex set in $\mathbb{R}^{N_{\boldsymbol{u}}}$, it can be proven that the EMS is a convex polytope in $\mathbb{R}^{N_{\boldsymbol{\nu}}}$ [25].

While it is always straightforward to associate every point in the ACS to its counterpart in the EMS, not all CA methods are capable of mapping the EMS in its entirety back to the ACS. For a given B matrix and given characteristics of the effectors, this is only dependent on the formulation of the CA problem and on the properties of the f_{CA} function. The subset of the EMS which a CA method can trace to feasible positions of the effectors is here referred to as the

AMS. The AMS is, in general, a subset of the EMS. Control objectives in the EMS which are outside of the AMS are unattainable by the given CA method, despite being actually attainable by the control power available to the aircraft.

For this reason, the present paper uses the volume of the AMS as a criterion to evaluate and compare the impact of different CA methods on top-level CS layout parameters. Three classic CA methods are compared in the present study. Their formulations and main properties are briefly introduced in the remainder of this section. A comprehensive and detailed overview of CA approaches and solution methods can be found in [26, 27]. Comparisons of different CA methods are also presented in [28], for a tailless aircraft, and in [29], for a BWB. Neither study is concerned with design and sizing of CS layouts.

A. Mechanical Gearing and Ganging

Gearing is here defined as the process of connecting the motion of one effector to the one of its input through a constant gearing ratio. Ganging is instead defined as the process of constraining the relative motion among two or more actual effectors, hence defining a subset of virtual effectors. A ganging matrix G can be designed to establish a linear relationship between the real effectors $\boldsymbol{u}$ and the virtual ones $\overline{\boldsymbol{u}}$, as shown in Equation 4.

$$\boldsymbol{u} = G\overline{\boldsymbol{u}} \tag{4}$$

If the number of virtual effectors is equal to the number of control objectives $\boldsymbol{\nu}$, the displacement of real effectors can be determined simply by matrix inversion, as shown in Equation 5.

$$\boldsymbol{\nu} = B\boldsymbol{u} = BG\overline{\boldsymbol{u}} \Rightarrow \overline{\boldsymbol{u}} = (BG)^{-1}\boldsymbol{\nu} \tag{5}$$

Ganging control effectors and gearing them to the pilot stick are possible ways to model a mechanical linkage between the pilot inputs and the effectors displacement. Gearing and ganging matrices need to be selected *a priori* and somewhat arbitrarily, and usually need to be optimized for different flight scenarios. Furthermore, while it can be rather intuitive to gang effectors on a conventional aircraft, it may not be so straightforward for unconventional aircraft geometries.

The ganging operation is usually employed to link control effectors such that they can affect each motion axis independently. In fact, the capability of an effector to control multiple motion axes at the same time can be seen as an unwanted coupling effect, as in the case of adverse yaw dynamics triggered by the deployment of ailerons. On the other hand, it can also be a beneficial source of available control power, if exploited properly. For this purpose, more advanced CA techniques need to be introduced.

B. Constrained Pseudo Inverse

The CPI method solves the optimization problem reported in the following Equation 6, resulting in the minimum-norm feasible effectors displacements required to achieve the control objective $\boldsymbol{\nu}$. This problem does not admit an analytical solution, and it must be solved via an iterative algorithm.

$$\begin{aligned} \min_{\boldsymbol{u}} \quad & \boldsymbol{u}\boldsymbol{u}^T \\ \text{s.t.} \quad & B\boldsymbol{u} - \boldsymbol{\nu} = 0 \\ & \boldsymbol{u}_{\text{lb}} \leq \boldsymbol{u} \leq \boldsymbol{u}_{\text{ub}} \end{aligned} \tag{6}$$

It is well known that the AMS of the CPI method is smaller than the actual EMS, and it can be proven that this is always the case for all CA methods based on generalized inverse matrices [24]. For this reason, this type of approaches is usually defined as sub-optimal. On the other hand, CA methods based on generalized inverses are usually easier to solve and more robust. For this reason, they have already been implemented in some advanced operations [30].

C. Direct Allocation

The Direct Control Allocation (DCA) method has been explicitly conceived on the basis of the geometric representation of the EMS itself. By definition, the AMS of the DCA coincides with the EMS, and the method is defined as optimal [24]. The DCA method is usually formulated as the optimization problem shown in Equation 7, where the auxiliary variable $\boldsymbol{w} \equiv \boldsymbol{u}$ is used to indicate the candidate solution, and the scale factor ρ is used to evaluate the control

objectives in the same direction of $\boldsymbol{\nu}$.

$$\begin{aligned} \max_{\rho,\boldsymbol{w}} \quad & \rho \\ \text{s.t.} \quad & B\boldsymbol{w} = \rho\boldsymbol{\nu} \\ & \boldsymbol{u}_{\text{lb}} \leq \boldsymbol{w} \leq \boldsymbol{u}_{\text{ub}} \end{aligned} \tag{7a}$$

$$\begin{cases} \boldsymbol{u} = \boldsymbol{w}/\rho, & \text{if } \rho > 1 \\ \boldsymbol{u} = \boldsymbol{w}, & \text{if } 0 \leq \rho \leq 1 \end{cases} \tag{7b}$$

In its most computationally efficient formulation, DCA is cast as a linear programming problem, hence also relying on an iterative algorithm for its solution [27].

III. Methodology

The applications presented in this paper aim at minimizing the total span dedicated to CSs, for a fixed number of CSs, with an assigned and constant chord ratio, and under the constraints of desired FQs performance. The latter are evaluated through flight dynamics simulation, with the aircraft FCS employing an assigned CA method. A multi-disciplinary optimization framework has been developed to assess the impact of different CA methods on top-level CS layout parameters. This is achieved by iteratively reducing the span of each CS in a given layout, and by exploring different layouts entirely. The requirement of small CS spans, together with a contained number of CSs themselves, is usually desired to reduce system complexity, reduce weight, and/or reserve more space for high-lift devices [19, 31]. The architecture of the optimization framework is shown in Figure 2, in the form of an Extended Design Structure Matrix (XDSM) [32]. The main components of the optimization framework are described in the following subsections.

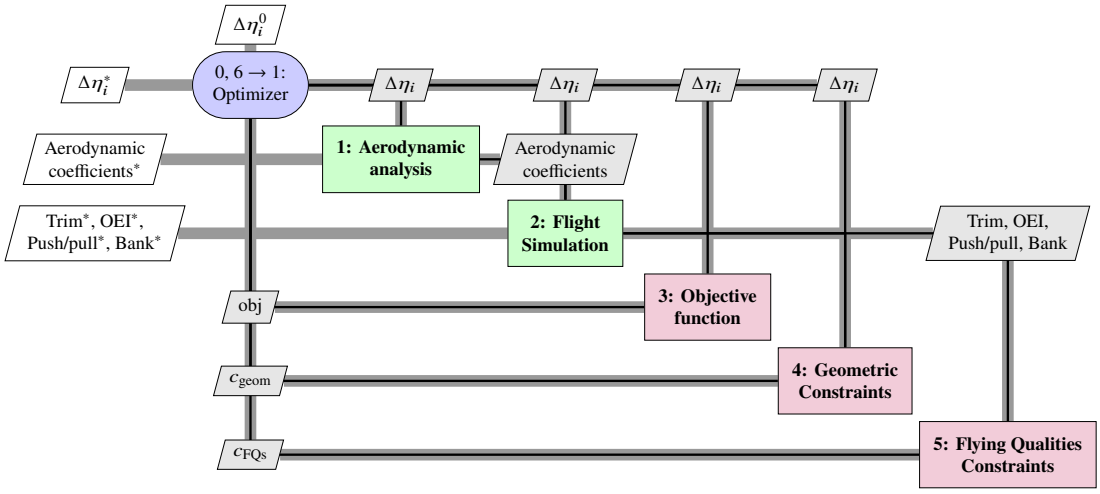

Fig. 2 Extended Design Structure Matrix (XDSM) of the proposed optimization framework.

A. Optimization problem

The formal expression of the optimization problem is reported in Equation 8. The CS spans $\Delta\eta_i$, nondimensionalized with respect to the aircraft full wing span, have been chosen as design variables. Chord ratios are assigned and held fixed, as well as the number of CSs.

$$
\begin{aligned}
\min_{\Delta\eta_i} \quad & \sum_{i=1}^{N_{\mathrm{CS}}} \Delta\eta_i && && (8)\\
\text{s.t.} \quad & \left|\eta_i^{\mathrm{out}}\right| > \left|\eta_i^{\mathrm{in}}\right| && \forall i = 1, 2, ..., N_{\mathrm{CS}} \\
& \left|\eta_i^{\mathrm{out}}\right| < \left|\eta_{i+1}^{\mathrm{in}}\right| && \forall i = 1, 2, ..., N_{\mathrm{CS}} - 1 \\
& \Delta\eta_i^{\min} \leq \Delta\eta_i \leq \Delta\eta_i^{\max} && \forall i = 1, 2, ..., N_{\mathrm{CS}} \\
& C_{\mathrm{FQs}}
\end{aligned}
$$

Spans are subject to a combination of geometric bounds and constraints which prevent CSs to overlap, exceed assigned maximum and minimum span limits, and clash with other airframe elements such as the vertical tails intersection with the rear wing (as in the case of Figure 1) or wing-podded engines (if present). Moreover, the inboard station of each inboard CS is held fixed, as well as the outboard station of each outboard CS. In this way each CS span is altered by moving only the side of the CS which is closer to the middle of the wing. This approach anchors each CS to its position within the layout, and is necessary to prevent the whole CSs from moving towards the middle of the wing section, which is a space reserved for high-lift devices.

FQs constraints are evaluated through non-linear flight dynamics simulations, where CS deflections are determined by the CA method under investigation. Since the aim of this work is to compare the impact of different CA methods on CS layout parameters, only FQs criteria focused on aircraft controllability are considered. The following criteria have been reproduced from [33], and their outcome has been evaluated against the corresponding Level 1 requirements for Category III transport aircraft:

- Trim in straight and level flight. The aircraft must be trimmable at a given flight condition. This test is assumed successful if the magnitude of residual accelerations after trim is lower than $\left\|\boldsymbol{a}^{\mathrm{lim}}\right\| = 1 \times 10^{-6}\,\mathrm{m/s^2}$.
- Push/pull maneuver. Full longitudinal stick deflections must result in normal load factors of at least $n_z^{\mathrm{lim}} = 2.0$ for a pull-up maneuver, and $n_z^{\mathrm{lim}} = 0.5$ for a push-down maneuver.
- Time to bank. A full lateral deflection of the stick must result in a roll angle of $\varphi^{\mathrm{lim}} = 30°$ within a time span of $\Delta t_\varphi^{\mathrm{lim}} = 2.3\,\mathrm{s}$.
- One Engine Inoperative (OEI) conditions. The aircraft must be trimmable in asymmetric conditions with one engine being inoperative.

For each criterion, the limit value which guarantees Level 1 FQs is used to formulate and normalize the constraint inequalities. These are summarized in Equation 9.

$$
C_{\mathrm{FQs}} = \begin{cases}
\left\|\boldsymbol{a}^{\mathrm{tr}}\right\| \leq \left\|\boldsymbol{a}^{\mathrm{lim}}\right\| & \text{for each trim FQs test} \\
n_z^{\max} \geq n_z^{\mathrm{lim}} & \text{for each pull-up FQs test} \\
n_z^{\min} \leq n_z^{\mathrm{lim}} & \text{for each push-down FQs test} \\
\Delta t_\varphi \leq \Delta t_\varphi^{\mathrm{lim}} & \text{for each time-to-bank FQs test}
\end{cases} \tag{9}
$$

FQs criteria are evaluated in cruise and approach conditions, and for two different cross-wind speeds, according to the experiment matrix reported in Table 1. The cross-wind magnitude is set as $V_w = 25\,\mathrm{kts}$, as prescribed in current certification regulations for commercial aircraft [34].

The problem is solved using the sequential quadratic programming algorithm within the `fmincon` function in MATLAB. This solver satisfies bound constraints at all iterations, which is important to protect the aerodynamic solver from infeasible CS sizes. Additionally, it is able to handle unconverged and infinite function values, making it possible to recover from untrimmmable flight conditions. The solver stops either by reaching an optimality tolerance of 10^{-6} or a step size of 10^{-2}. All bounds and constraints are respected with a tolerance of 10^{-6}.

Table 1 FQs test matrix used as constraints for the optimization study. Aircraft mass and CG are assigned before each test.

		Cruise	**Approach**
No wind	$V_w = 0$ kts	Trim, Push/pull, Time to bank	Trim, Push/pull, Time to bank, OEI trim
Cross-wind	$V_w = 25$ kts	Trim, Push/pull	Trim, Push/pull, OEI trim

B. Aerodynamic analysis

For a given CS layout and sizing iteration, the aerodynamic force and moment coefficients are expressed as a tabular function of the angle of attack, angle of sideslip, Mach number, angular rates, and CS deflections. The aerodynamic model consists of a linear superposition of three components: the steady contribution of the clean airframe, the quasi-steady contributions due to angular rates, and the differential contributions due to CS deflections. Its formal expression is reported in Equation 10.

$$C_F = C_{F_0}(\alpha, \beta, M, \boldsymbol{\delta} = \mathbf{0}) + \sum_{\omega=p,q,r} \frac{\partial C_F}{\partial \omega}(\alpha, \beta, M, \boldsymbol{\delta} = \mathbf{0})\omega \; + \sum_{i=1}^{N_{\text{CS}}} \Delta C_F(\alpha, \beta, M, \delta_i) \tag{10}$$

Such model disregards possible interaction effects between CSs and assumes linear dependence of the aerodynamic actions on the angular rates. The differential actions due to CS deflections are determined by subtraction of the clean, steady coefficients from the ones obtained with a single CS deflected. This approach decouples the aerodynamic models for the clean airframe and its CSs. Nevertheless, it is deemed acceptable for a conceptual/preliminary design study.

The Athena Vortex Lattice (AVL) solver has been chosen to perform the large number of aerodynamic analyses required for the optimization study [35]. This linear solver approximates surfaces using two-dimensional quadrilateral panels, and allows rapid evaluation of a given flight condition with acceptable accuracy for the present application. On the other hand, the 2D assumption restricts the validity of the aerodynamic analysis to thin structures. For this reason, only the lifting surfaces are included in the analysed geometry model, while the influence of the fuselage is neglected.

To reduce computational time even further, a simple database feature is implemented to store the tabular data of the differential aerodynamic actions of each CS on the basis of the wing it belongs to, its span wise position and its span. These data can be directly retrieved if the optimization of Equation 8 needs to re-evaluate a certain combination of the aforementioned parameters, without the need to perform a new AVL analysis.

C. Flight Mechanics and Control

Dynamic simulations aimed at evaluating FQs criteria are performed in the Performance, Handling Qualities and Load Analysis Toolbox (PHALANX), developed in-house in the MATLAB/Simulink environment. PHALANX is a modular toolbox for non-linear, six degrees of freedom flight simulation and analysis [22]. It integrates variable-fidelity models to describe aerodynamics, propulsive system, mass and inertia properties of a multi-body system, and provides functionalities to design arbitrary FCS architectures.

The toolbox has been used in several previous studies on novel aircraft configurations like the Blended Wing Body [36], the Delft University Unconventional Configuration, featuring the propulsive empennage concept [37], and other box-wing aircraft [20, 21, 38]. An overview diagram of PHALANX is shown in Figure 3.

In the present framework, PHALANX is used to model an open-loop FCS with flexible architecture, taking inputs in the form of predefined pilot commands, and distributing them to CS deflections through different CA methods. This approach allows to evaluate the inherent FQs performance of an unaugmented flight mechanics model as a function of the chosen CA method. A block-scheme of the FCS architecture implemented in the present study is shown in Figure 4.

For the MGG method, pilot inputs are scaled, mixed through a constant ganging matrix and routed to the effectors. For the CPI and DCA methods, pilot inputs are first transformed into demanded control moments through Non-linear Dynamic Inversion (NDI) [39, 40], which are then allocated to CS deflections with the respective CA algorithm [24]. In the latter two cases, pilot inputs are interpreted as desired angular accelerations in body axes, and the aerodynamic moments that are due to the bare airframe contributions are assumed to be measured perfectly by the FCS.

In all cases, control inputs to the effectors are passed through a second-order actuator model with a natural frequency of 30 rad/s, a damping ratio of 0.7, a rate limit of 45 °/s and saturation limits of ±30°.

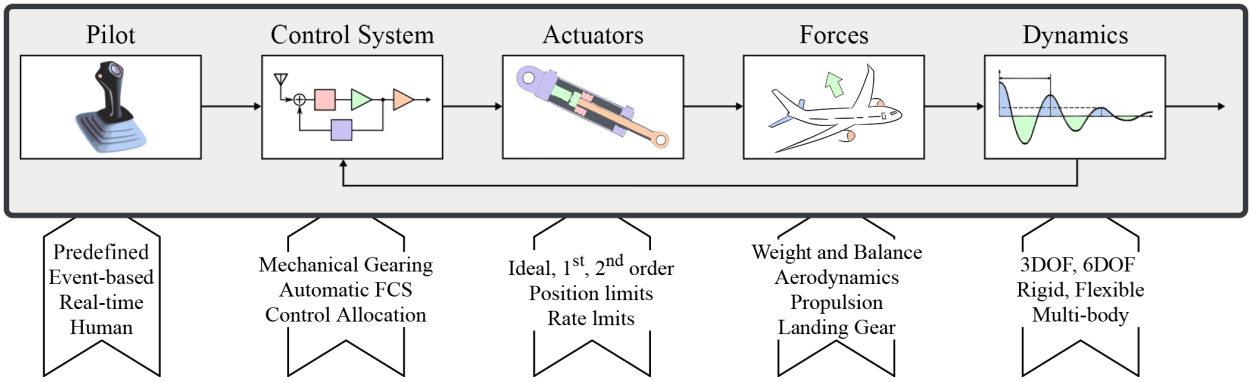

Fig. 3 Top-level overview of the PHALANX flight mechanics model.

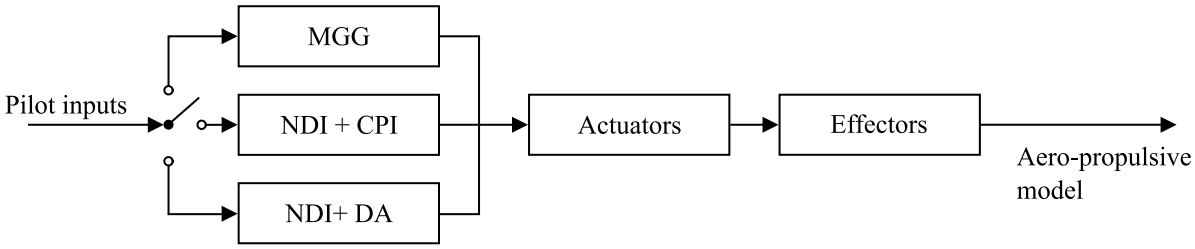

Fig. 4 Block scheme overview of the FCS architecture with variable architecture.

IV. Applications and Results

Two main applications have been carried out in this work. The first one, presented in Section IV.A, compares the minimum cumulative CS span obtained with each of the MGG, CPI and DCA methods for the most traditional box-wing CS layout according to literature [17–19]. The second one, presented in Section IV.B, explores a novel CS layout for staggered box-wings, featuring a CS close to the central section of the rear wing, outside of the twin vertical tail region. A synthetic overview of both applications is reported in Table 2.

Table 2 Overview of the application studies proposed in Section IV.

	Purpose	**CA methods**	**CS layouts**
Section IV.A	Impact of CA methods on minimum CS span	MGG, CPI, DCA	Traditional [17–19]
Section IV.B	Exploration of new CS layouts for box-wing aircraft	DCA	Traditional. Traditional + central rear CS. Traditional with inboard rear CS replaced by central rear CS.

For both applications, the staggered box-wing geometry represented in Figure 5 has been used as the clean baseline airframe. This model is based on the early design of a box-wing aircraft referred to as the PrandtlPlane (PrP), and developed within the PARSIFAL* project. The cruise condition has been defined as $M = 0.79$ and $h = 11$ km, on the basis of mission requirements from the PARSIFAL project. The approach condition has been chosen as $V = 120$ kts and $h = 0$ km, on the basis of typical values for comparable commercial transport aircraft. For both cruise and approach flight conditions, the airframe mass has been assumed as $m = 115\,000$ kg, which corresponds to fuel tanks being at 75% of their total capacity. The position of the CG is such that a 10% static margin is achieved in cruise conditions This position is kept fixed through each optimization, for both cruise and approach flight scenarios. This assumption is deemed realistic, in light of the limited CG excursion achievable by using fuel trim for box-wing aircraft [41].

*Prandtlplane ARchitecture for the Sustainable Improvement of Future AirpLanes (PARSIFAL), `https://parsifalproject.eu/`

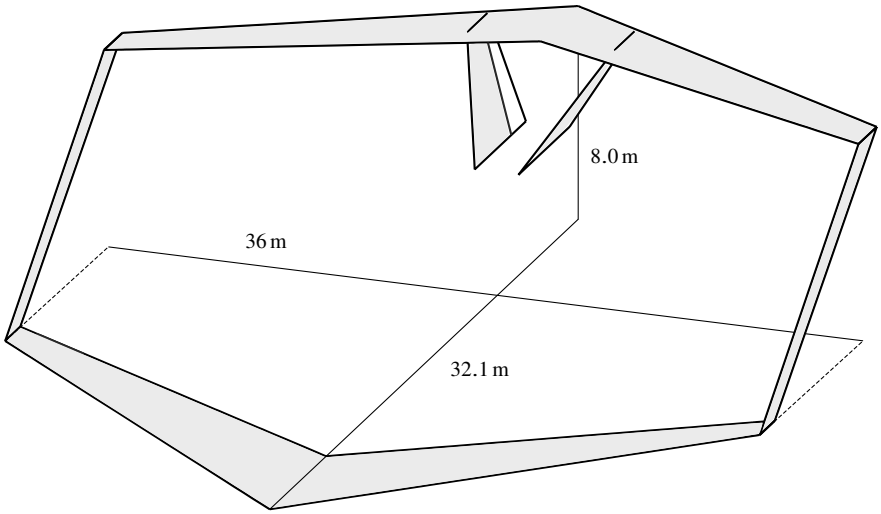

Fig. 5 Staggered box-wing geometry under investigation.

The inner stations of the inboard CSs are fixed, as well as the outer stations of the outboard ones. Thus, the optimizer only operates on the outer stations of the inboard CSs, and on the inner stations of the outboard ones. The rudders on the V-tail are assumed fixed in size, and hence not included in the CS sizing process. All CSs are assigned a constant chord fraction of 0.3, and are given a small clearance to other geometrically constraining elements, such as the fuselage (of the complete aircraft), wing tips, or the wing-tail intersection.

On the front wing, the space in between the two CSs is occupied by a plain flap, which is set to a deflection of 30° for approach and 0° for cruise. The span wise position and size of this flap are not design variables, but follow from the adjacent CSs sizes. It is assumed that there are no requirements on the airfield performance that would pre-determine a certain flap size or type. Instead, the optimization problem formulated as in Equation 8 will result in the set of CSs with the smallest total span and, as a consequence, in the largest possible flaps.

A. Impact of Control Allocation methods on Control Surface spans

This study compares the minimum cumulative CS span obtained with each of the MGG, CPI and DCA methods, under the same FQs constraints, for the most traditional box-wing CS layout in literature [17–19]. Such a layout features one Inboard (I) and one Outboard (O) CS on each of the Front (F) and Rear (R) wings. It is shown in Figure 6, with a visualization of how each CS span can be altered by the optimizer.

Since compliance with the same set of FQs is guaranteed by the optimization framework described in Section III, the optimum total CS span is used to compare the performance of the CA methods. A sensitivity study on initial conditions is performed. A detailed discussion is provided on the correlation between the CS span distribution and the properties

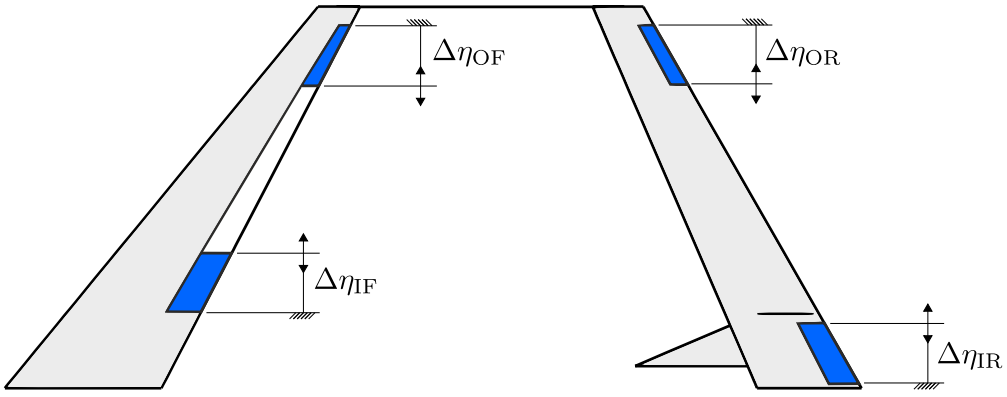

Fig. 6 Top-view of the traditional box-wing CS layout, with visualization of how each CS span can be altered by the optimizer.

Table 3 Initial values and bound constraints for the CS spans.

Study	$\Delta\eta_{\mathrm{IF}}$	$\Delta\eta_{\mathrm{OF}}$	$\Delta\eta_{\mathrm{IR}}$	$\Delta\eta_{\mathrm{OR}}$	$\Delta\eta_i^{\min}$	$\Delta\eta_i^{\max}$
1	0.08	0.08	0.08	0.08	0.01	0.10
2	0.08	0.06	0.08	0.06	0.01	0.10
3	0.06	0.08	0.06	0.08	0.01	0.10

of the AMS that the optimum layout is capable to achieve by using each CA method.

The optimization study has been performed three times for each CA method, with different combinations of initial CS spans. The initial values and bound constraints for the CS spans are shown in Table 3. In all cases, the initial CSs are all large enough to assure good FQs and provide the optimizer a feasible, yet improvable solution. The lower bound was specified to prevent any CS from degenerating into a segment, hence compromising the consistency of the layout. The upper bound was set to limit the design space, in accordance with preliminary investigations which showed that larger values of the CS span are not necessary.

For the MGG method, front and rear inboard CSs operate as elevators moving in phase opposition only in response to pitch commands. The outboard surfaces deflect as ailerons only in response to lateral commands, and the rudders are constrained to deflect together, acting as pure yawing moment generators. The ganging matrix used in this case is reported in the following Equation 11. For the other CA methods, all CSs on the main wings operate independently, while rudders are treated in the same way as before.

$$\boldsymbol{u} = \begin{bmatrix} 0 & 0 & 0 & 0 & 0 & 0 & 0 & 0 & 1 & 1 \\ 1 & 1 & 0 & 0 & -1 & -1 & 0 & 0 & 0 & 0 \\ 0 & 0 & -1 & 1 & 0 & 0 & -1 & 1 & 0 & 0 \end{bmatrix}^T \begin{Bmatrix} \overline{u}_{\mathrm{ail}} \\ \overline{u}_{\mathrm{ele}} \\ \overline{u}_{\mathrm{rud}} \end{Bmatrix}, \quad \text{with}$$
$$\boldsymbol{u} = \left\{ u_{\mathrm{IF}}^{\mathrm{left}}, u_{\mathrm{IF}}^{\mathrm{right}}, u_{\mathrm{OF}}^{\mathrm{left}}, u_{\mathrm{OF}}^{\mathrm{right}}, u_{\mathrm{IR}}^{\mathrm{left}}, u_{\mathrm{IR}}^{\mathrm{right}}, u_{\mathrm{OR}}^{\mathrm{left}}, u_{\mathrm{OR}}^{\mathrm{right}}, u_{\mathrm{rud}}^{\mathrm{left}}, u_{\mathrm{rud}}^{\mathrm{right}} \right\}^T \tag{11}$$

Results are graphically reported in Figures 7 and 8. The conventional MGG approach requires the largest overall CS widths. This is expected, since roll and pitch moments are only achieved by delegated CSs. The CPI method is able to use all effectors in combination, hence reducing the total required span by about 9.5%. Lastly, DCA reduces the required span even further, achieving a reduction of about 17% compared to MGG.

As shown in Figure 7a, the individual optimum CS spans achieved with MGG are very similar for all tested initial conditions. The main differences lie in the distribution between the front and rear inner surfaces, but a certain consistency can be clearly observed. On the other hand, both CPI and DCA result in relevant differences between the optimum CS spans, as shown in Figure 7b and Figure 7c, respectively. For each CA method, the final values of the objective function are similar (within 3%) for all tested initial conditions, as shown in Figure 8.

Figure 9 correlates the total CS span with the volume of its AMS, for every CA method and initial layout, and shows the evolution of both variables during each optimization study. As explained in Section II, the volume of the AMS is a common measure to quantify the total control power that a CA method can provide for a given CS layout. For the optimal value of the total CS span, the different CA methods are seen forming clearly distinguishable clusters in the chart. The MGG cluster requires the largest total CS span, but only achieves an intermediate AMS volume. The CPI cluster presents smaller total CS width than the MGG, and achieves the minimum AMS volume overall. The DCA cluster requires the lowest total CS span, but achieves the largest AMS volume. This confirms that it is able to achieve the highest control power with the smallest CSs, making the most effective use of all CS sizes.

Inspecting the shape of the AMSs makes it possible to further analyze the performance of these CA methods. The three AMSs geometries are compared in Figure 10, in three dimensions, and in Figure 11, in two-dimensional views.

Overall, the AMS corresponding to the CPI and DCA layouts present a more rounded, oval-like shape, in comparison to the MGG method which results in a prismatic shape. This is especially true in the $(C_{\mathcal{L}}, C_{\mathcal{M}})$ plane and clearly identifies a smooth trade-off between the roll and pitch control power. This is in light of the fact that all CSs on the main wings are employed for control objectives along both of these axes. As the required control power increases about the roll axis, the available control power about the pitch axis decreases, and vice versa.

The opposite is true for the layout obtained with the MGG method, for which the $(C_{\mathcal{L}}, C_{\mathcal{M}})$ plane presents a rectangular shape. This is because the roll and pitch control tasks have been explicitly assigned to two independent

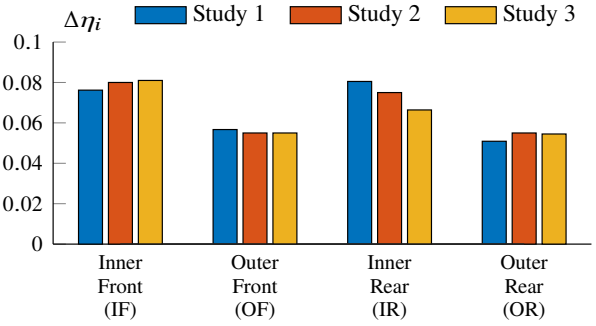

a) Mechanical Gearing and Ganging (MGG)

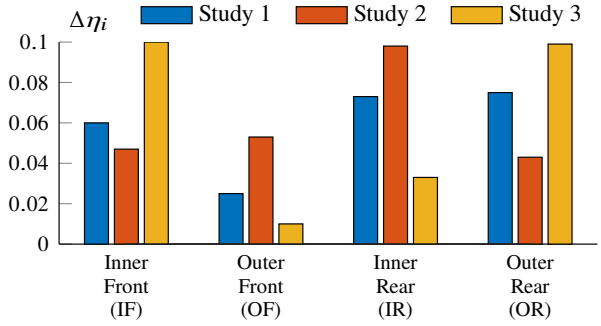

b) Constrained Pseudo-Inverse (CPI)

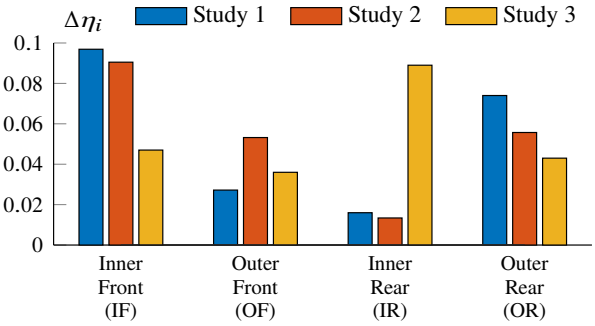

c) Direct Control Allocation (DCA)

Fig. 7 Comparison of optimal CS spans for different CA methods and initial conditions. The legend refers to the initial conditions reported in Table 3.

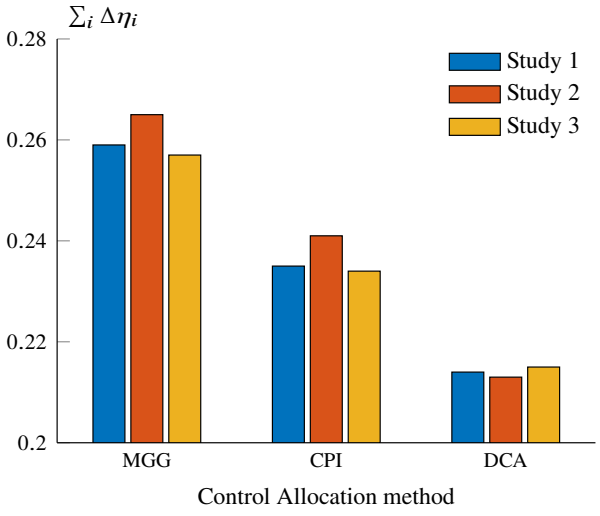

Fig. 8 Comparison of optimal cumulative CS spans for different CA methods and initial conditions. The legend refers to the initial conditions reported in Table 3.

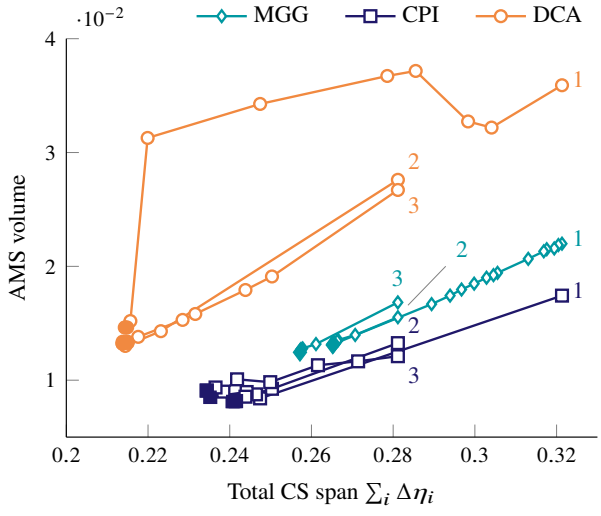

Fig. 9 Evolution of AMS volume and cumulative CS span with optimizer iterations, for different CA methods. Initial conditions at the respective number label, as reported in Table 3. Final iterations at filled markers.

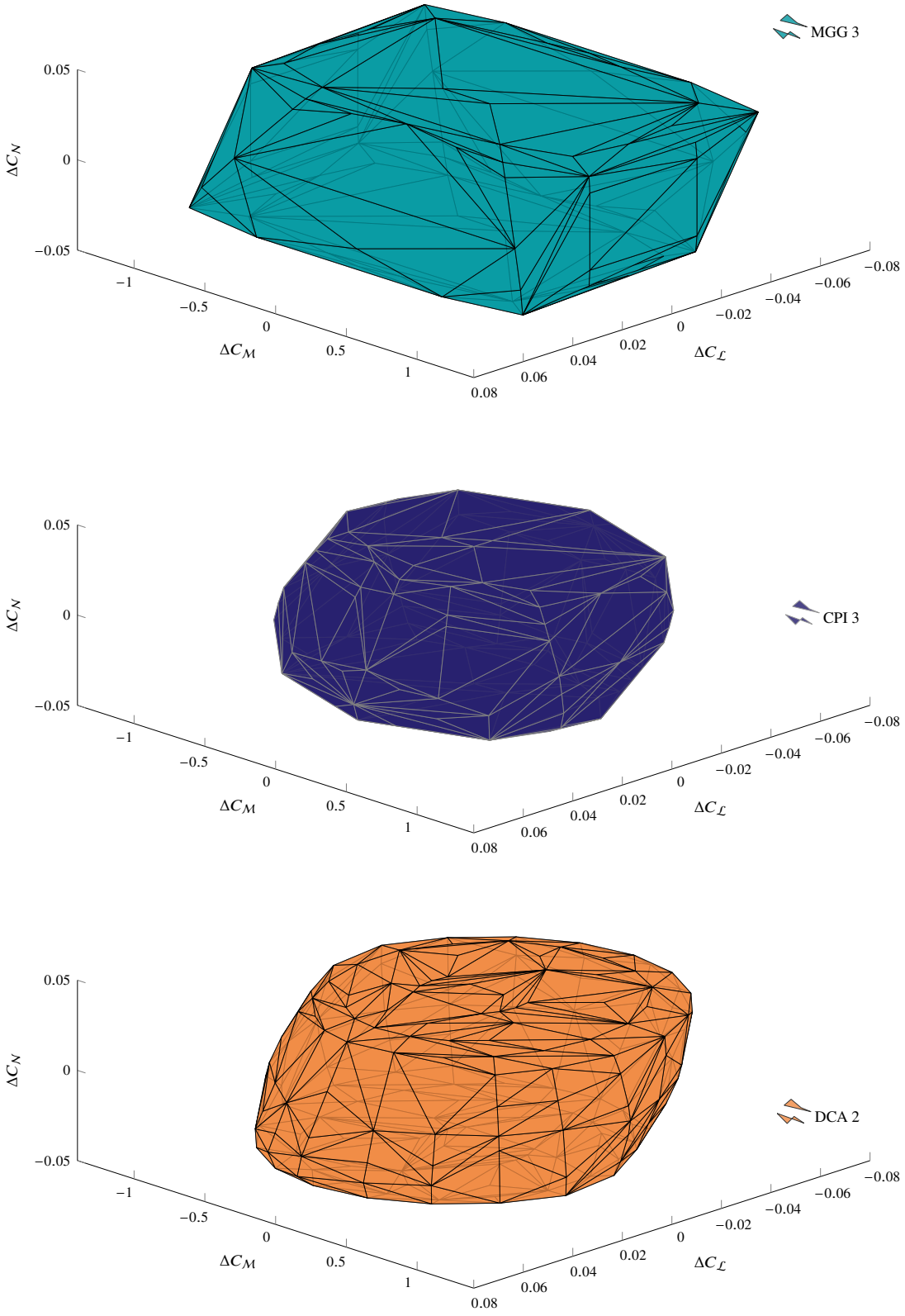

Fig. 10 Visualization of the AMSs corresponding to the optimal CS layouts obtained with each CA method. The legend entry refers to the CS layouts reported in Figure 8.

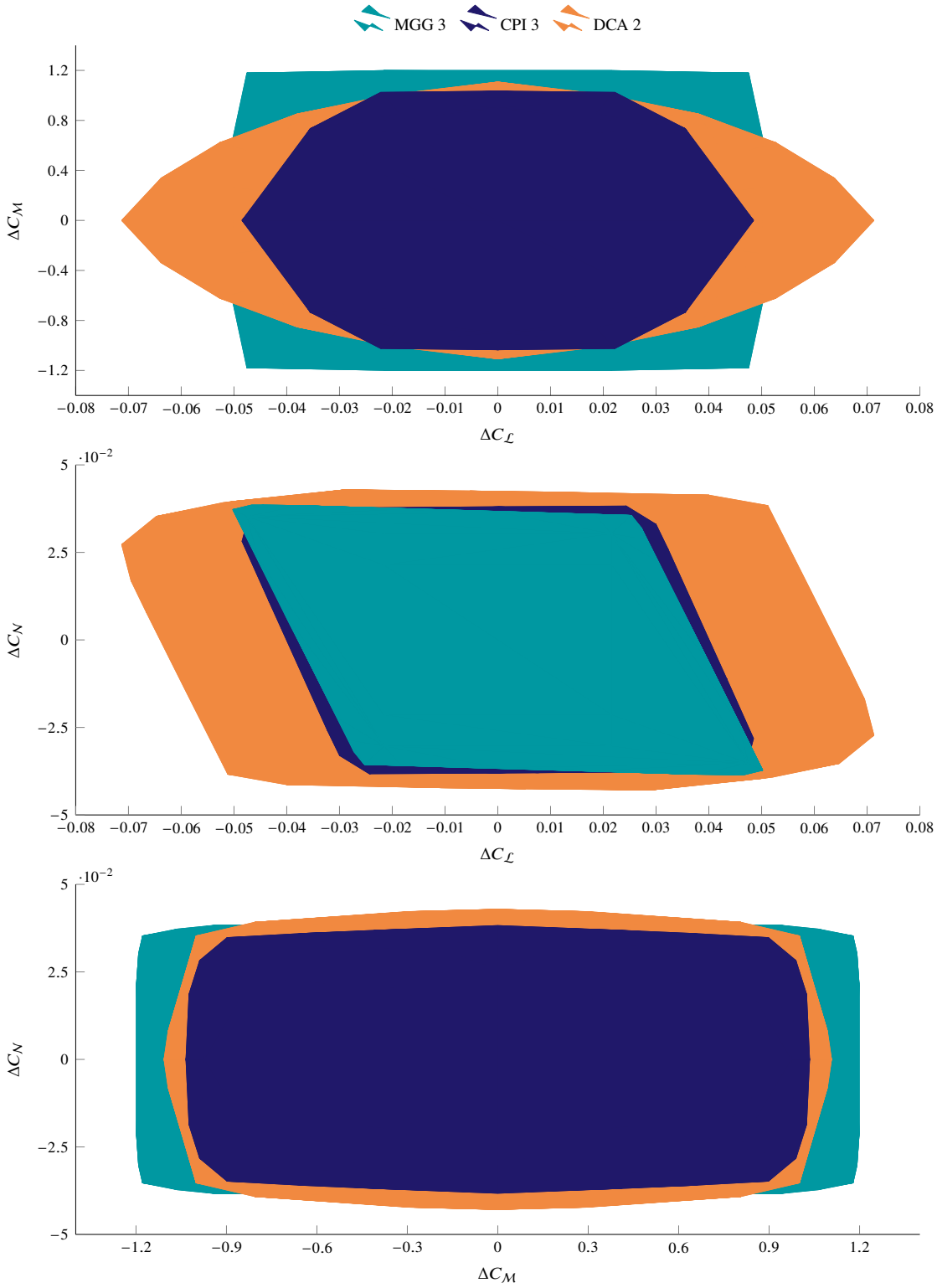

Fig. 11 Comparison of the AMSs corresponding to the optimal CS layouts obtained with each CA method. Legend entries refer to the CS layouts reported in Figure 8.

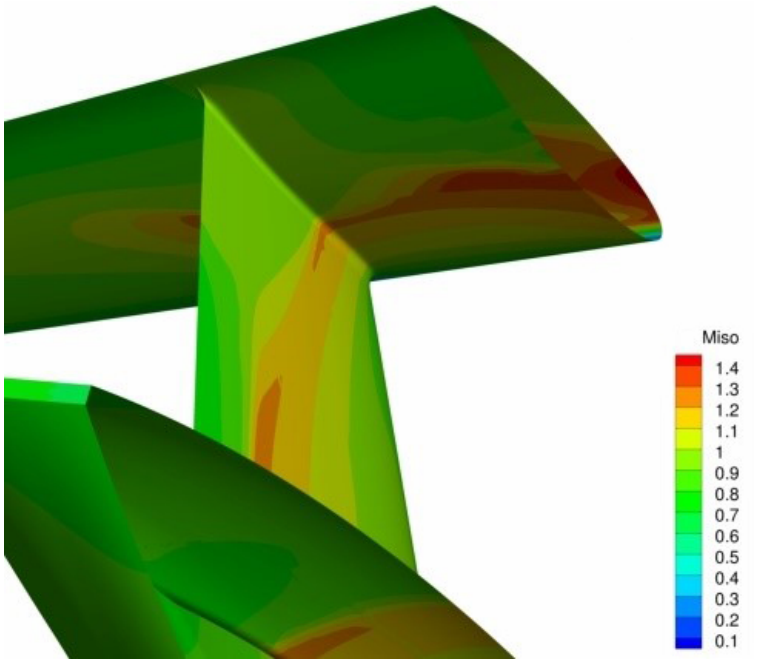

Fig. 12 Isentropic Mach number distribution at the junction between the vertical tail and the rear wing of a staggered box-wing aircraft in cruise conditions ($M = 0.79$, $Re = 25.86 \times 10^6$, $h = 11$ km, $\alpha = 0$ deg) [42].

sets of CSs. The latter behavior can also be observed in the $(C_{\mathcal{M}}, C_{\mathcal{N}})$ plane for all three layouts, since pitch and yaw moment generation are fundamentally uncoupled in the current setup. Lastly, a small coupling due to adverse yaw is visible in the $(C_{\mathcal{L}}, C_{\mathcal{N}})$ plane for all three methods.

The maximum extension of all three AMSs along the yaw axis is comparable for all three layouts, since yaw control effectiveness is mainly ascribed to rudders, which have not been included in the design optimization problem. The AMSs corresponding to the optimal layout of the MGG and CPI methods are basically overlapping in the $(C_{\mathcal{L}}, C_{\mathcal{N}})$ plane. On the other hand, the AMS of the layout obtained with DCA is significantly more extended along the roll axis. The AMS of the MGG method is the most extended one along the pitch axis, although the difference with the other methods is smaller in this case.

B. Exploration of novel Control Surface layouts

This application explores novel CS layouts for staggered box-wings, featuring a CS close to the central section of the rear wing, outside of the twin vertical tail region. In light of its capability to achieve maximum control power with minimum control span, the DCA method is now used to optimize three different initial layouts for the rear wing. Namely:

Layout A is the one studied in the previous section, now used as a benchmark. It features an Inboard (I) CS, between the two vertical tails, and an Outboard (O) CS, close to the wing tip.

Layout B features an Inboard (I) CS between the two vertical tails, an Outboard (O) CS close to the wing tip, and one extra "Central" (C) CS, close to the mid-wing section and outside of the vertical tail region;

Layout C features only the aforementioned "Central" (C) CS, and an Outboard (O) CS, close to the wing tip.

For all three layouts, the CSs on the front wing retain the same arrangement as in the previous study. The central CS, when present on the rear wing, is treated as an inboard one, since its inner station is constrained by the wing-tail intersection.

The interest in exploring the use of a CS outside of the vertical tail region is motivated by Figure 12. For a staggered box-wing aimed at transonic applications, the flow field around the wing-tail intersection is complex and conducive to shock waves and strong aerodynamic interactions. These have a detrimental effect on interference drag and overall performance, as well as on control surface effectiveness. In order to avoid additional complications due to the deflection of movable devices, it would be desired to position CSs in regions of the wing which enjoy a more predictable and effective flow field.

This design goal is explored with Layouts B and C. Layout B serves to evaluate how control authority is redistributed when the CS in the problematic inboard location can be aided by an additional CS. It has one CS more than Layout A and Layout C, and its set of CSs is the union of the ones of the other two layouts. Layout C serves the same purpose, but evaluates the performance of the layout when the CS in the problematic inboard location is entirely removed and relocated to the mid-wing region. It has the same number of CSs as Layout A.

The three layouts with initial and final CS spans are shown in Figure 13. Results from the three optimization studies are summarized in Figure 14 and Table 4.

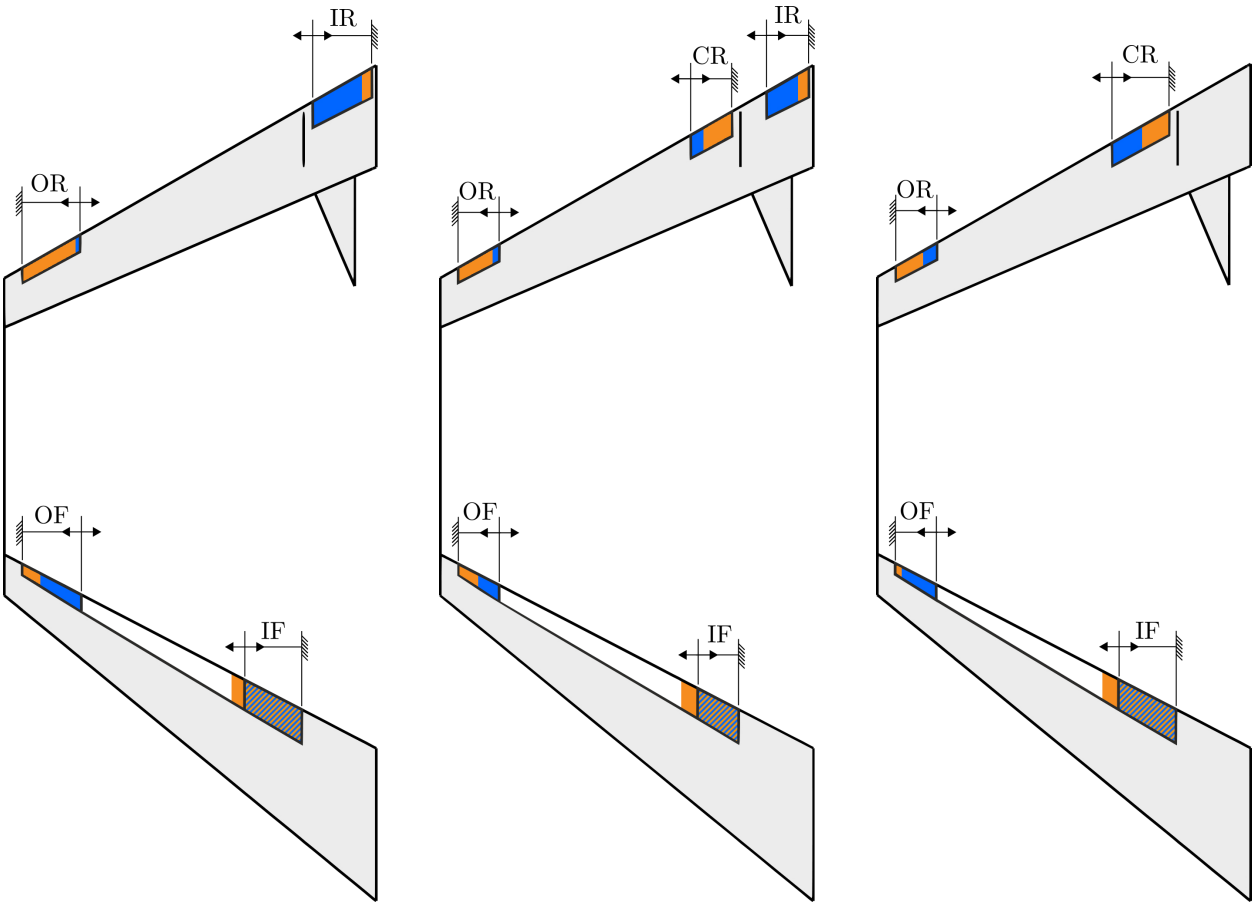

a) Layout A **b)** Layout B **c)** Layout C

Fig. 13 Top view of CS Layouts A, B and C. Spans are to scale and correspond to the assigned initial values (in blue), and optimum final values using DCA (in orange).

With respect to Layout A, Layout B shows a 2.3% reduction in total CS span, which is likely to be too little to justify (and compensate for) the presence of one extra movable surface. On the other hand, Layout C achieves about 13% decrease in the same parameter, while making use of one less movable than Layout B. This is due to the fact that the inner rear CS (between the vertical tails) has been completely replaced by the one close to the mid-wing section (CR), outside of the vertical tail region, whose position allows contributing more flexibly to both roll and pitch maneuvers, effectively behaving like an elevon.

For Layout B, the center rear CS achieves approximately the same span of its counterpart in Layout C. Despite both the inner front and outer rear CSs being slightly smaller than in Layout A, their reduction is not sufficient to justify the addition of an extra CS. For Layout C, the rear CSs are equal in span, while the outer front CS is reduced to its minimum allowed size. This shows how the center rear CS is very effective for both pitch and roll control, and can thus result in lower total span.

Lastly, it is interesting to note how the optimizer retains certain CSs on both the front and rear wing for all final layouts. The inner front and the outer rear CSs, together with the center rear CS (when present), seem to be the most

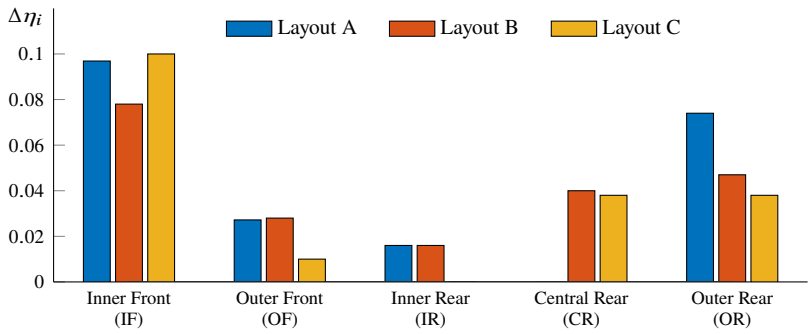

Fig. 14 CS span comparison among Layouts A, B and C.

Table 4 Optimum cumulative CS span for Layouts A, B and C, with comparison to Layout A.

Layout	$\sum_i \Delta\eta_i$	Δ%
A	0.214	—
B	0.209	-2.3%
C	0.186	-13.1%

important ones, as they are never reduced to a span smaller than $\Delta\eta = 0.038$. The outer front and the inner rear CSs become extremely small and ineffective in all the layouts where they appear, with the former reaching the minimum bound value for its span in Layout C. This suggests that they could probably be removed from the layout altogether, in favor of increased simplicity of its architecture. Replacing the inner rear CS with a central one has indeed proved worthy, in light of the results achieved with Layout C. Analogous investigations can be conducted for the outer front CS in the future.

V. Conclusions

The paper has compared Control Surface (CS) layouts designed and sized to obtain the same Flying Qualities (FQs) performance with different Control Allocation (CA) methods. It has also proposed novel CS layouts for staggered box-wing aircraft aimed at transonic flight. All design tasks have been performed through a general, physics-based, configuration-agnostic, multi-disciplinary optimization framework. The optimization problem has been formulated to obtain CS layouts with minimum cumulative span, while complying with desired FQs performance constraints, for a specified set of flight scenarios in approach and cruise conditions.

The original contribution of the work, a summary of the obtained results, and suggestions for future research are highlighted in the following sections.

A. Original contribution

Flying qualities have been calculated by using a modular, fully non-linear flight mechanics model. A variable-architecture flight control system has made it possible to assess them as a function of different CA methods, for the same airframe. This has allowed to compare the impact of a conventional Mechanical Gearing and Ganging (MGG) kinematic chain, a Constrained Pseudo-Inverse (CPI) CA method, and a Direct Control Allocation (DCA) method on the design and sizing of different CS layouts of a staggered box-wing. This approach advances the current state of the art in CS layout design for box-wings, as the only CA method applied in literature so far is the conventional MGG kinematic chain, which is used in this work as a benchmark.

With the proposed methodology, a novel CS layout has been discovered for staggered box-wings. It has been found that the cumulative CS span required by staggered box-wing aircraft to achieve good FQs performance can be significantly reduced if the inboard rear CS (inside the twin tail region) is completely replaced by a mid-wing CS positioned outside of the twin tail region. By employing the DCA method, the mid-wing surface can aid in both longitudinal and lateral flight maneuvers, hence functioning as a proper elevon and providing both roll and pitch control power. This is a novel result, as no previous study on box-wing configurations has ever considered such CS layout, either with or without the employment of more advanced CA methods. The newly proposed layout is also expected to avoid undesired interactions with the twin tail region, which can present complex aerodynamic phenomena especially in transonic regime.

B. Summary of results

Results have shown the benefits of employing CA methods already at conceptual/preliminary design stage. The CS layout obtained by employing DCA proves superior, according to the selected objective function, to the same layout

obtained with the conventional MGG, used ubiquitously in the literature. Results have also shown that CA methods with non-analytical solutions make the design space complex, and allow for different local minima with comparable optimal values of the total CS span. The decision to employ such CA methods for aircraft operations should hinder the a priori choice of a specific CS layout to achieve prescribed FQs performance.

For the box-wing configuration presented in the paper, the MGG method is the most suitable to attain all combinations of coupled moments, in light of its reliance on independent sets of CSs. On the other hand, it does need the largest CS span to satisfy all FQs constraints. The CPI method manages to be effective for all of the FQs tests that do not require strongly coupled moments, but it needs extra CS span, as compared to the DCA method, to satisfy the FQs requirements in presence of side-wind. As the DCA method accesses the entire Effective Moment Set (EMS) of its respective layout, it results in the largest moment-generation capabilities and obtains the smallest total CS span overall. For this reason, DCA should be the prime choice for control systems of aircraft configurations with redundant CSs, such as multi-wing or box-wing aircraft.

C. Recommendations

Continuing on the present work, a higher fidelity aerodynamic model is advised to include effects of the fuselage, as well as non-linear effects due to deflections/interactions of CSs. This is especially relevant for the front wing, where relatively small CSs interact with high-lift devices. Moreover, the actual need for outer front CSs should be further investigated, since the outer rear ones seem to be always preferred by the optimizer when employing DCA.

Further research should generalize the proposed framework by also including stability considerations, as well as flight scenarios such as take-off and landing. In the design iteration, this would introduce a coupling between the spans of flaps and CSs, which could be tackled by prescribing a supplementary set of FQs performance requirements. Lastly, it would be interesting to compare layouts obtained with different design objectives, such as minimum control surface area, minimum required actuator power, or maximum Attainable Moment Set (AMS) volume.

Funding sources

The research presented in this paper has been carried out in the framework of the PARSIFAL (Prandtlplane ARchitecture for the Sustainable Improvement of Future AirpLanes) research project, which has been funded by the European Union within the Horizon 2020 Research and Innovation Program (Grant Agreement n.723149).

References

[1] Gudmundsson, S., Cattaneo, M., and Redondi, R., "Forecasting temporal world recovery in air transport markets in the presence of large economic shocks: The case of COVID-19," *Journal of Air Transport Management*, 2020.

[2] Airbus, "Global Market Forecast," Tech. rep., Airbus SE, 2019. URL `https://www.airbus.com/aircraft/market/global-market-forecast.html`.

[3] Directorate General for Research and Innovation, Directorate General for Mobility and Transport, "Flightpath 2050: Europe's Vision for Aviation," Tech. rep., European Commission, 2011. URL `https://ec.europa.eu/transport/sites/transport/files/modes/air/doc/flightpath2050.pdf`.

[4] Liu, Y., Elham, A., Horst, P., and Hepperle, M., "Exploring Vehicle Level Benefits of Revolutionary Technology Progress via Aircraft Design and Optimization," *Energies*, Vol. 11, No. 1, 2018, p. 166. https://doi.org/10.3390/en11010166.

[5] Okonkwo, P., and Smith, H., "Review of evolving trends in blended wing body aircraft design," *Progress in Aerospace Sciences*, Vol. 82, 2016, pp. 1–23. https://doi.org/10.1016/j.paerosci.2015.12.002.

[6] Martinez-Val, R., Perez, E., Alfaro, P., and Perez, J., "Conceptual design of a medium size flying wing," *Proceedings of the Institution of Mechanical Engineers, Part G: Journal of Aerospace Engineering*, Vol. 221, No. 1, 2007, pp. 57–66. https://doi.org/10.1243/09544100jaero90.

[7] Frediani, A., Rizzo, E., and Bottoni, C., "A 250 Passenger PrandtlPlane transport aircraft preliminary design," *Aerotecnica Missili & Spazio*, Vol. 84, No. 4, 2016, pp. 152–163.

[8] Frediani, A., Cipolla, V., and Oliviero, F., "IDINTOS: the first prototype of an amphibious PrandtlPlane-shaped aircraft," *Aerotecnica Missili & Spazio*, Vol. 94, No. 3, 2015, pp. 195–209. https://doi.org/10.1007/BF03404701.

[9] Andrews, S. A., and Perez, R. E., "Stability and Control Effects on the Design Optimization of a Box-Wing Aircraft," *14th AIAA Aviation Technology, Integration, and Operations Conference*, Atlanta, GA, 2014, p. 2592. https://doi.org/10.2514/6.2014-2592.

[10] Frediani, A., "The Prandtl Wing," *Von Kárman Institute for Fluid Dynamics: VKI Lecture Series: Innovative Configurations and Advanced Concepts for Future Civil Transport Aircraft.*, 2005.

[11] Prandtl, L., "Induced Drag of Multiplanes," Tech. Rep. 182, National Advisory Committee for Aeronautics, 1924.

[12] Munk, M., "Elements of the wing section theory and of the wing theory," Tech. Rep. 191, National Advisory Committee for Aeronautics, 1924.

[13] Demasi, L., Monegato, G., Dipace, A., and Cavallaro, R., "Minimum Induced Drag Theorems for Joined Wings, Closed systems, and Generic Biwings: Theory," *56th AIAA/ASCE/AHS/ASC Structures, Structural Dynamics, and Materials Conference*, 2015. https://doi.org/10.2514/6.2015-0697.

[14] Abu Salem, K., Cipolla, V., Palaia, G., Binante, V., and Zanetti, D., "A Physics-Based Multidisciplinary Approach for the Preliminary Design and Performance Analysis of a Medium Range Aircraft with Box-Wing Architecture," *Aerospace*, Vol. 8, No. 10, 2021. https://doi.org/10.3390/aerospace8100292, URL https://www.mdpi.com/2226-4310/8/10/292.

[15] de Wringer, S., Varriale, C., and Oliviero, F., "A Generalized Approach to Operational, Globally Optimal Aircraft Mission Performance Evaluation, with Application to Direct Lift Control," *Aerospace*, Vol. 7, No. 9, 2020, p. 134. https://doi.org/10.3390/aerospace7090134.

[16] Sousa, A. N., de Paula, A. A., Ribeiro, F. C., and Cardoso-Ribeiro, F. L., "Box wing longitudinal flight quality evaluation," *AIAA Aviation 2019 Forum*, Dallas, Texas, 2019, p. 3490. https://doi.org/10.2514/6.2019-3490.

[17] Varriale, C., Raju Kulkarni, A., La Rocca, G., and Voskuijl, M., "A Hybrid, Configuration-agnostic Approach to Aircraft Control Surface Sizing," *Italian Association of Aeronautics and Astronautics XXV International Congress*, Rome, Italy, 2019, pp. 9–13.

[18] Oliviero, F., Zanetti, D., and Cipolla, V., "Flight dynamics model for preliminary design of PrandtlPlane wing configuration with sizing of the control surfaces," *Aerotecnica Missili & Spazio*, Vol. 95, No. 4, 2016, pp. 201–210. https://doi.org/10.1007/BF03404728.

[19] van Ginneken, D., Voskuijl, M., van Tooren, M., and Frediani, A., "Automated Control Surface Design and Sizing for the Prandtl Plane," *51st AIAA/ASME/ASCE/AHS/ASC Structures, Structural Dynamics, and Materials Conference*, Orlando, Florida, 2010, p. 3060. https://doi.org/10.2514/6.2010-3060.

[20] Varriale, C., and Voskuijl, M., "A Control Allocation approach to induce the center of pressure position and shape the aircraft transient response," *Aerospace Science and Technology*, Vol. 119, 2021. https://doi.org/10.1016/j.ast.2021.107092.

[21] Varriale, C., and Voskuijl, M., "A trim problem formulation for maximum control authority using the Attainable Moment Set geometry," *CEAS Aeronautical Journal*, 2021. https://doi.org/10.1007/s13272-021-00560-4.

[22] Varriale, C., "Flight Mechanics and Performance of Direct Lift Control: Applying Control Allocation Methods to a Staggered Box-Wing Aircraft Configuration," phdthesis, Delft University of Technology, 2022. https://doi.org/10.4233/uuid:8b868c52-f34f-4307-8fc0-b1176eaf9d04.

[23] Durham, W. C., "Constrained control allocation," *Journal of Guidance, Control, and Dynamics*, Vol. 16, No. 4, 1993, pp. 717–725.

[24] Durham, W., Bordignon, K. A., and Beck, R., *Aircraft Control Allocation*, John Wiley & Sons, Ltd, Chichester, UK, 2016. https://doi.org/10.1002/9781118827789.

[25] Bordignon, K. A., "Constrained control allocation for systems with redundant control effectors," phdthesis, Virginia Tech, 1996. URL http://hdl.handle.net/10919/28570.

[26] Johansen, T. A., and Fossen, T. I., "Control allocation—A survey," *Automatica*, Vol. 49, No. 5, 2013, pp. 1087–1103. https://doi.org/10.1016/j.automatica.2013.01.035.

[27] Bodson, M., "Evaluation of Optimization Methods for Control Allocation," *Journal of Guidance, Control, and Dynamics*, Vol. 25, No. 4, 2002, pp. 703–711. https://doi.org/10.2514/2.4937.

[28] Buffington, J., "Tailless aircraft control allocation," *Guidance, Navigation, and Control Conference*, 1997, p. 3605. https://doi.org/10.2514/6.1997-3605.

[29] Waters, S. M., Voskuijl, M., Veldhuis, L. L., and Geuskens, F. J., "Control allocation performance for blended wing body aircraft and its impact on control surface design," *Aerospace Science and Technology*, Vol. 29, No. 1, 2013, pp. 18–27. https://doi.org/10.1016/j.ast.2013.01.004.

[30] Bordignon, K., and Bessolo, J., "Control Allocation for the X-35B," *2002 Biennial International Powered Lift Conference and Exhibit*, American Institute of Aeronautics and Astronautics, 2002. https://doi.org/10.2514/6.2002-6020.

[31] Dussart, G. X., Lone, M. M., and O'Rourke, C., "Size Estimation Tools for Conventional Actuator System Prototyping in Aerospace," *AIAA Scitech 2019 Forum*, American Institute of Aeronautics and Astronautics, 2019, p. 1634. https://doi.org/10.2514/6.2019-1634.

[32] Lambe, A. B., and Martins, J. R. R. A., "Extensions to the design structure matrix for the description of multidisciplinary design, analysis, and optimization processes," *Structural and Multidisciplinary Optimization*, Vol. 46, No. 2, 2012, pp. 273–284. https://doi.org/10.1007/s00158-012-0763-y.

[33] US Department of Defense, "Flying Qualities of Piloted Airplanes," Mil-f-8785c handbook, US Department of Defenses, 1969.

[34] EASA, "Certification Specifications for Large Aeroplanes CS-25A19," Tech. rep., European Aviation Safety Agency, 2017.

[35] Drela, M., and Youngren, H., *AVL 3.36 User Primer*, MIT Aero & Astro, 2 2007.

[36] Voskuijl, M., La Rocca, G., and Dircken, F., "Controllability of Blended Wing Body Aircraft," *26th Congress of International Council of the Aeronautical Sciences*, 2008.

[37] Varriale, C., Hameeteman, K., Voskuijl, M., and Veldhuis, L. L., "A Thrust-Elevator Interaction Criterion for Aircraft Optimal Longitudinal Control," *AIAA Aviation 2019 Forum*, American Institute of Aeronautics and Astronautics, 2019, p. 3001. https://doi.org/10.2514/6.2019-3001.

[38] Voskuijl, M., de Klerk, J., and van Ginneken, D., "Flight Mechanics Modeling of the PrandtlPlane for Conceptual and Preliminary Design," *Springer Optimization and Its Applications*, Springer US, 2012, pp. 435–462. https://doi.org/10.1007/978-1-4614-2435-2_19.

[39] Miller, C., "Nonlinear Dynamic Inversion Baseline Control Law: Architecture and Performance Predictions," *AIAA Guidance, Navigation, and Control Conference*, American Institute of Aeronautics and Astronautics, 2011, p. 6467. https://doi.org/10.2514/6.2011-6467.

[40] Lombaerts, T., Kaneshige, J., Schuet, S., Aponso, B. L., Shish, K. H., and Hardy, G., "Dynamic Inversion based Full Envelope Flight Control for an eVTOL Vehicle using a Unified Framework," *AIAA Scitech 2020 Forum*, American Institute of Aeronautics and Astronautics, 2020, p. 1619. https://doi.org/10.2514/6.2020-1619.

[41] Piet, R., "Preliminary design and analysis of fuel systems for box wing aircraft," Msc thesis, Delft University of Technology, 2022. URL http://resolver.tudelft.nl/uuid:3a2cf648-a7ef-498d-923d-f0b12f90595f.

[42] Carini, M., Méheut, M., Sanders, L., Kanellopoulos, S., Varriale, C., La Rocca, G., Abu Salem, K., Cipolla, V., and Binante, V., "Aerodynamic and Acoustic Analysis of the baseline PrandtlPlane," techreport PARSIFAL Deliverable 4.1, Office National d'Etudes et de Recherches Aérospatiales (ONERA), Delft University of Technology, University of Pisa, SkyBox Engineering, 2020. URL https://www.parsifalproject.eu/PARSIFAL_DOWNLOAD/PARSIFAL_D41.pdf.